Inorganica Chimica Acta 454 (2017) 240–246

Contents lists available at ScienceDirect

Inorganica Chimica Acta

journal homepage: www.elsevier.com/locate/ica

Research paper

Synthesis, characterisation and dynamic behavior of photoactive bipyridyl ruthenium(II)-nicotinamide complexes

Nichola A. Smith [a], Pingyu Zhang [a], Luca Salassa [b,c,d], Abraha Habtemariam [a], Peter J. Sadler [a,*]

[a] Department of Chemistry, University of Warwick, Gibbet Hill Road, Coventry CV4 7AL, UK
[b] CIC biomaGUNE, Paseo de Miramón 182, Donostia-San Sebastián, 20009, Spain
[c] Kimika Fakultatea, Euskal Herriko Unibertsitatea and Donostia International Physics Center (DIPC), P.K. 1072, Donostia-San Sebastián 20080, Spain
[d] Ikerbasque, Basque Foundation for Science, Bilbao 48011, Spain

ARTICLE INFO

Article history:
Received 27 April 2016
Received in revised form 4 June 2016
Accepted 6 June 2016
Available online 7 June 2016

Keywords:
Dynamic behavior
Polypyridyl Ru(II) complexes
Nicotinamide
NMR
DFT

ABSTRACT

The synthesis, characterization and dynamic behavior of three complexes, *cis*-[Ru(bpy)$_2$(NA)Cl][PF$_6$] (**1**), *cis*-[Ru(bpy)$_2$(NA)I][PF$_6$] (**2**) and *cis*-[Ru(bpy)$_2$(NA)$_2$][PF$_6$]$_2$ (**3**), where bpy is 2,2′-bipyridine, NA is nicotinamide are reported. These were designed as potential photoactivated antibacterial agents. Their dynamic behavior in solution was explored using NMR to probe the presence of atropisomers. The data show that the NA ligand in the *bis*-NA complex **3** rotates freely at 298 K on the NMR timescale; however, NA rotation in the mono-Cl and mono-I complexes **1** and **2** is hindered at the same temperature. DFT calculations suggested that this hindered rotation is due to hydrogen bonding between the NA protons closest to the nitrogen of the pyridine ring and the halide ligand. Interestingly Cl hinders rotation more than I, which corresponds to hydrogen bonding ability. Such dynamic behavior may influence the recognition of polypyridyl ruthenium drugs by biological targets.

1. Introduction

Administered drugs have to pass through many organs and cells before they reach their target sites, being exposed to different cell components and enzymes that can deactivate them [1]. In some cases, before a drug can interact with a biomolecule it needs to undergo a chemical reaction, i.e. it is a 'pro-drug'. For example, the anticancer agent cisplatin hydrolyses to provide binding sites for biomolecules such as DNA [2]. Thus to optimise the pharmacological activity of metal-based agents, it is important to understand their behavior in solution.

The most common targets for drugs are either proteins (e.g. enzymes, receptors) or nucleic acids (e.g. DNA), and a drug can bind to such targets either by a direct reaction and thus covalent (or coordinative in the case of metals) bonding, or weak interactions involving intermolecular bonds (e.g. hydrogen bonding, hydrophobic interactions) [3]. It is well known that cisplatin binds to DNA, and its binding properties have been extensively studied [4]. Octahedral Ru(II) complexes, such as [Ru(azpy)$_2$Cl$_2$], where azpy is 2-(phenylazo)pyridine, have been shown to be cytotoxic to breast cancer cell lines [5]. Since DNA is an important target, the addition of benzimidazole ligands (to simulate the binding of nucleic acids) to form *cis*-[Ru(azpy)$_2$(MeBim)$_2$]$^{2+}$, where MeBim is methylybenzimidazole, was investigated and the rotation behavior of MeBim was explored [6]. A similar analysis was also carried out for *cis*-[Ru(bpy)$_2$(MeBim)$_2$]$^{2+}$, concluding that more sterically-demanding ligands rotate more slowly [7]. Atropisomers occur in compounds in which rotation about a single bond is hindered. Is it an important area of drug design, as different atropisomers can have different binding affinities towards targets and thus exhibit different activities [8–11].

This paper is focussed on two Ru(II) polypyridyl mono-halido complexes, *cis*-[Ru(bpy)$_2$(NA)X]$^+$, and the *bis*-substitued Ru(II) polypyridyl complex, *cis*-[Ru(bpy)$_2$(L)$_2$]$^{2+}$, where bpy is 2,2′-bipyridine, NA is nicotinamide and X is Cl or I (Fig. 1). These nicotamide complexes are potential photoactivatable antibacterial agents which might act as delivery vehicles for the organic antibacterial ligand nicotamide as well as reactive Ru(II) polypyridyl fragments. Here we report their synthesis and characterization as well as their dynamic behavior in solution investigated by NMR spectroscopy and DFT calculations. In the case of complexes **1** and **2**, the rotation of NA was hindered on the NMR timescale at ambient temperature, a behavior that was surprisingly not observed for complex **3**. The hindered rotation was explored by computational methods (DFT) which revealed that hydrogen bonding between the halide ligand and protons of the NA ligand cause the hindered rotation.

* Corresponding author.
E-mail address: p.j.sadler@warwick.ac.uk (P.J. Sadler).

http://dx.doi.org/10.1016/j.ica.2016.06.014
0020-1693/

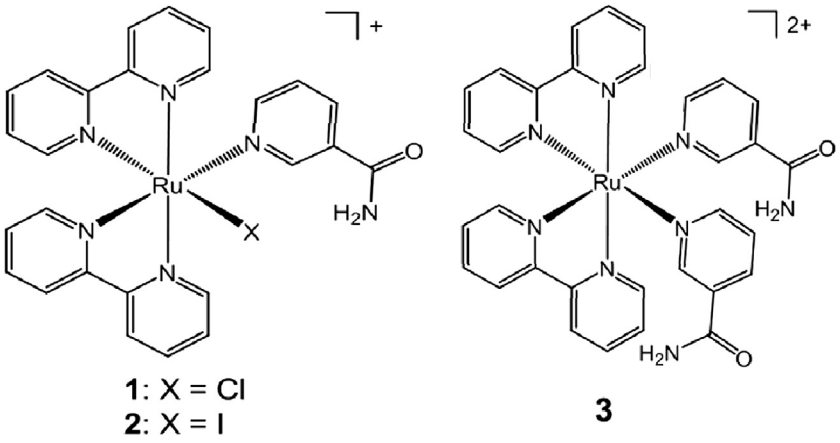

Fig. 1. General structure of the complexes studied in this work.

2. Experimental

2.1. Materials

Nicotinamide (NA) and NH_4PF_6 were purchased from Sigma-Aldrich and used without further purification. The *cis*-[Ru(bpy)$_2$(X)$_2$] starting materials, X = Cl or I, were synthesised as described previously [12,13]. The NMR spectroscopy solvents acetone-d^6 and DMSO-d_6 were purchased from Cambridge Isotope Laboratories Inc, and D_2O from Sigma-Aldrich.

2.2. Preparation of Ru(II) polypyridyl complexes

2.2.1. *cis*-[Ru(bpy)$_2$(NA)Cl][PF$_6$] (**1**)

A solution of *cis*-[Ru(bpy)$_2$(Cl)$_2$] (104 mg, 0.2 mmol) and nicotinamide (NA) (30 mg, 0.24 mmol) was stirred in 25 mL 1:4 v/v water:ethanol for 8 h at 75 °C before it turned from light red to dark red. A dark precipitate was obtained after addition of NH_4PF_6 (163 mg, 1 mmol). Yield 82% (118 mg, 0.16 mmol). Elemental analysis calculated for $C_{26}H_{22}ClF_6N_6OPRu{\cdot}0.5H_2O$ %C: 43.09, %H: 3.20, %N: 11.59; found %C: 42.26, %H: 2.86, %N: 11.34. ESI-MS calculated for $C_{26}H_{22}ClN_6ORu$ $[M]^+$ *m/z* 571.1, found *m/z* 570.9. ^{1}H NMR (acetone-d^6, 500 MHz) δ H: 6.9 (1H, NH), 7.3 (1H, ddd, *J* = 7.6, 5.5 and 1.2 Hz), 7.4 (1H, ddd, *J* = 7.6, 5.6 and 1.2 Hz), 7.5 (1H, t, *J* = 7.0), 7.6(1H, NH), 7.7 (1H, ddd, *J* = 7.7, 5.5 and 1.2 Hz), 7.8 (1H, d, *J* = 5.7 Hz), 7.9 (1H, ddd, *J* = 7.6, 5.5 and 1.1 Hz), 7.9 (2H, m), 8.1 (1H, d, *J* = 5.7 Hz), 8.2 (2H, m), 8.3 (1H, dt, *J* = 7.9 and 1.5 Hz), 8.6 (1H, d, *J* = 8.1 Hz), 8.6 (1H, d, *J* = 8.2 Hz), 8.6 (1H, d, *J* = 8.1 Hz), 8.7 (1H, d, *J* = 5.6 Hz), 8.7 (1H, d, *J* = 8.1 Hz), 9.1 (2H, br s), 10.1 (1H, d, *J* = 5.6 Hz).

2.2.2. *cis*-[Ru(bpy)$_2$(NA)I][PF$_6$] (**2**)

A solution of *cis*-[Ru(bpy)$_2$(I)$_2$] (250 mg, 0.35 mmol) and nicotinamide (NA) (50 mg, 0.42 mmol) was stirred in 25 mL 1:4 v/v water:ethanol for 8 h at 75 °C before it turned from light red to dark red. A dark precipitate was obtained after addition of NH_4PF_6 (280 mg, 0.17 mmol). Yield 35% (100 mg, 0.12 mmol). Elemental analysis calculated for $C_{26}H_{22}IF_6N_6OPRu{\cdot}H_2O$ %C: 37.77, %H: 2.26, %N: 10.17; found %C: 37.69, %H: 2.22, %N: 10.14. ESI-MS calculated for $C_{26}H_{22}IN_6ORu$ $[M]^+$ *m/z* 663.0, found *m/z* 662.9. ^{1}H NMR (acetone-d^6, 500 MHz) δ H: 6.9 (1H, NH), 7.3 (1H, t, *J* = 6.6 Hz), 7.4 (2H, m), 7.5 (1H, NH), 7.8 (1H, t, *J* = 6.6 Hz), 7.9 (2H, m), 8.0 (2H, m), 8.0 (1H, d, *J* = 5.8 Hz), 8.2 (2H, m), 8.3 (1H, d, *J* = 7.9 Hz), 8.5 (1H, d, *J* = 8.1 Hz), 8.6 (1H, d, *J* = 8.0 Hz), 8.6 (1H, d, *J* = 8.2 Hz), 8.8 (1H, d, *J* = 8.1 Hz), 8.9 (1H, d, *J* = 5.4 Hz), 9.3 (1H, br s), 9.3 (1H, br s), 10.6 (1H, d, *J* = 5.6).

2.2.3. *cis*-[Ru(bpy)$_2$(NA)$_2$][PF$_6$]$_2$ (**3**)

A suspension of *cis*-[Ru(bpy)$_2$(Cl)$_2$] (104 mg, 0.2 mmol) was stirred in 20 mL water at 80 °C before it turned to a red solution. Nicotinamide (NA) (122 mg, 1 mmol) was added and solution was heated to reflux for 2.5 h. The solution turned from red to deep red and NH_4PF_6 (163 mg, 1 mmol) was added. An orange precipitate was isolated. Yield 49% (92 mg, 97 μmol). Crystals suitable for X-ray crystallography were obtained from a saturated aqueous solution at 277 K. Elemental analysis calculated for $C_{32}H_{28}F_{12}N_8O_2P_2Ru$ %C: 40.56, %H: 2.98, %N: 11.82, found %C: 40.25, %H: 2.91, %N: 11.48. ESI-MS calculated for $C_{32}H_{28}N_8O_2Ru$ $[M]^{2+}$ *m/z* 329.1, found *m/z* 328.9. ^{1}H NMR (acetone-d^6, 500 MHz) δ H: 7.0 (2H, NH), 7.6 (6H, m), 8.0 (2H, ddd, *J* = 7.8,5.6 and 1.3 Hz), 8.1 (2H, td, *J* = 7.9 and 1.4 Hz), 8.3 (4H, m), 8.4 (2H, dt, *J* = 8.0 and 1.5 Hz), 8.6 (2H, d, *J* = 8.1 Hz), 8.7 (2H, d, *J* = 8.0 Hz), 8.9 (2H, d, *J* = 5.6 Hz), 9.0 (2H, s), 9.4 (2H, d, *J* = 5.7 Hz).

2.2.4. NMR of nicotinamide (NA)

^{1}H NMR (acetone-d^6, 400 MHz) δ H: 6.9 (1H, NH), 7.5 (1H, dd, *J* = 8.0 and 4.9 Hz), 7.7 (1H, NH), 8.3 (1H, dt, *J* = 8.0 and 1.9 Hz), 8.7 (1H, dd, *J* = 4.9 and 1.5 Hz), 9.1 (1H, d, *J* = 1.8 Hz).

2.3. Dynamic behavior studied by variable temperature ^{1}H NMR

500 MHz ^{1}H NMR spectra of Ru(II) polypyridyl complexes **1**, **2** and **3** in acetone-d^6 were obtained initially at 10–30 K intervals from 185 to 323 K on a Bruker AV-500 spectrometer using 5 o.d. NMR tubes. The concentration of each sample was 2.5 mg in 600 μL of NMR solvent (c.a. 6 mM). To obtain accurate coalescence temperatures (T_c) for **1** and **2**, the intervals were lowered to 2 K around the coalescence point. All data processing was carried out using Bruker Topspin 2.1. By using Eq. (1) the rate constant for exchange at coalescence (k_c) between states of an unequally populated two-site system can be found, where X is a value taken from tabulated values for various population (P) differences ($\Delta P = (P_1 - P_2)$) and Δ_v is the difference in resonance frequency of the exchanging protons [14–16]. The free energy of activation ($v\Delta G_c^{\neq}$) was calculated using Eq. (2), where a is a constant with a value of 1.914×10^{-2} kJ mol^{-1} [14]. NOESY spectra were obtained at 185 K using a mixing time of 0.8 s.

$$k_c = \frac{\pi_v}{X} \tag{1}$$

$$\Delta G_c^{\neq} = aT_c + \left[10.319 + \log\left(\frac{T_c}{k_c}\right)\right] \tag{2}$$

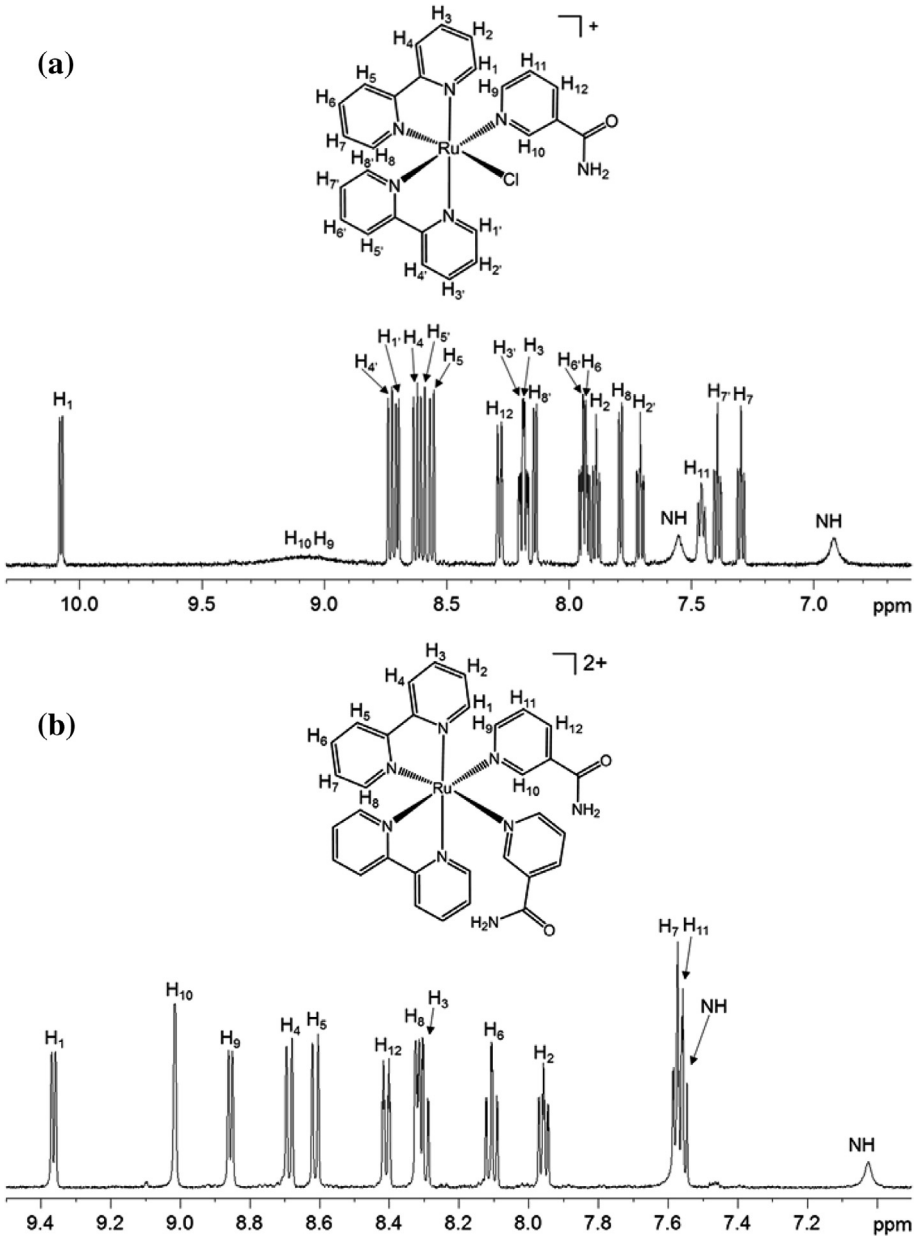

Fig. 2. 500 MHz ^{1}H NMR spectra of (a) *cis*-[Ru(bpy)$_2$(NA)Cl][PF$_6$] (**1**) and (b) *cis*-[Ru(bpy)$_2$(NA)$_2$][PF$_6$]$_2$ (**3**) in acetone-d^6 at 298 K.

2.4. Solvent effect on dynamic behavior studied by ^{1}H NMR

The effect of solvent on the dynamic behavior of Ru(II) polypyridyl complexes **1** and **2** was studied by recording 400 MHz ^{1}H NMR spectra at 298 K in acetone-d^6 and DMSO-d_6 on a Bruker DPX-400 spectrometer using 5 o.d. NMR tubes. The concentration of each sample was 2.5 mg in 600 μL of deuterated solvent (c.a. 6 mM).

2.5. Dynamic behavior studied by DFT

DFT geometry optimisations for complexes **1**–**3** were performed using Gaussian 03 in the gas phase [17]. Becke's three-parameter hybrid functional [18] with Lee-Yang-Parr's gradient-corrected correlation functional (B3LYP) [19] was used. The LanL2DZ basis set [20] and effective core potential were used for the ruthenium atom, and the split valence 3-21G basis set [21] was used for all other atoms. The nature of all stationary points was confirmed by normal mode analysis. A relaxed potential energy surface scan was performed using the B3LYP/LanL2DZ/3-21G optimised geometry to find a potential transition state using the same functional/basis set. The dihedral angle between the monodentate ligand (L) and the ruthenium atom was adjusted in intervals of 20° to simulate the rotation of nicotinamide (NA) in complexes [Ru(bpy)$_2$(NA)X]$^+$, where X is Cl or I. Geometry optimisation of the transition states was performed using B3LYP/LanL2DZ/3-21G as above. All B3LYP/LanL2DZ/3-21G geometries were then re-optimised using B3LPY/LanL2DZ/6-31G**+ and PB1PBE [22] /LanL2DZ/6-31G**+; the LanL2DZ basis set and effective core potential was used for the ruthenium and halide, and the split valence 6-31G**+ basis set [23] used for all other atoms. The DFT free energy of activation ($\Delta G^{\neq}_{DFT}$), i.e. energy of the rotational barrier, was calculated by taking the difference between total energy of the starting geometry (E_S) and total energy of the transition state (E_T), see Eq. (3).

$$\Delta G^{\neq}_{DFT} = E_T - E_S \quad (3)$$

3. Results and discussion

3.1. Synthesis and characterization

The monocationic Ru(II) polypyridyl halido complexes, *cis*-[Ru(bpy)$_2$(NA)Cl][PF$_6$] (**1**) and *cis*-[Ru(bpy)$_2$(NA)I][PF$_6$] (**2**), were synthesised by the reaction of the appropriate *cis*-[Ru(bpy)$_2$(Cl/I)$_2$] starting material with 1.2–1.3 mol equiv of NA in a mixture of 1:4 v/v water:ethanol. The complexes were fully characterised by ^{1}H NMR spectroscopy in acetone-d^6. For the chlorido complex **1**, there was one doublet at 10.1 ppm (H$_1$, bpy), which was low-field-shifted to 10.6 ppm for the iodido complex *cis*-[Ru(bpy)$_2$(NA)I][PF$_6$] **2**. The spectrum of **1** is shown in Fig. 2a. An interesting feature at ca. 9–9.5 ppm for complexes **1** and **2** is a broad peak that can be attributed to protons H$_9$ and H$_{10}$ on the monodentate NA that are in close proximity to the nitrogen of the pyridine ring. Both protons appear to be involved in an exchange processes at 298 K, attributed to the lack of COSY and NOE cross peaks in ^{1}H–^{1}H spectra of **1** at 298 K, see Fig. S1. This rate (on the NMR timescale) of conformational exchange can be attributed to the hindered rotation of the NA ligand.

The dicationic *bis*-substituted Ru(II) polypyridyl complex, *cis*-[Ru(bpy)$_2$(NA)$_2$][PF$_6$]$_2$ (**3**), was synthesised by the reaction of the appropriate *cis*-[Ru(bpy)$_2$(Cl)$_2$] starting material with a 5 mol equiv of nicotinamide (NA) in water. The complexes were fully characterised by ^{1}H NMR spectroscopy. In contrast to complexes **1** and **2**, the ^{1}H NMR resonance peaks for **3** were sharp and the number of proton peaks observed is reduced because of the symmetric nature of complex **3**, see Fig. 2b.

Table 1
Parameters determined for complexes **1** and **2** from variable temperature ^{1}H NMR experiments in acetone-d^6.

Complex	Δ_v (s^{-1})	k_c (s^{-1})	T_c (K)	$\Delta G_c^{\neq}$ (kJ mol^{-1})
1	688	1144	278	51.6 ± 0.2
2	598	994	256	47.7 ± 0.3

3.2. Dynamic behavior studied by variable temperature ^{1}H NMR

Variable temperature ^{1}H NMR spectroscopy was used to investigate the exchange behavior in complexes **1** and **2**. For complex **1**, heating the sample to 323 K, the broad peaks at 9–9.5 ppm were defined enough to show two broad peaks, see Fig. 3a and b. Interestingly for **2** the broad peaks at 9–9.5 ppm were relatively sharper and more defined upon heating at 323 K. When the samples of **1** and **2** were cooled to 185 K, two atropisomers were detected (denoted as Conf. 1 and Conf. 2, Fig. 3c). Again the atropisomers were assigned by investigating the NOE interaction between H$_{10}$/H$_9$ with H$_1$/H$_8$ (Fig. 3d). The chemical shift difference between H$_{10}$ and H$_9$ for both atropisomers of **1** (1.04 ppm for Conf. 1 and 1.71 ppm for Conf. 2) was greater than for **2** (0.9 ppm for Conf. 1 and 1.49 ppm for Conf. 2), see Table S1. For both **1** and **2**, the atropisomer with greatest chemical shift difference for H$_{10}$ and H$_9$ was Conf. 2. The chemical shift difference between H$_{10}$ and H$_9$ for both **1** and **2** was greater than that of the free ligand (0.4 ppm for NA). For both **1** and **2**, Conf. 1 was more stable in solution, with the ratio of Conf. 1 to Conf. 2 being 1:0.8. By using Eq. (2), the experimental free energy of activation ($\Delta G_c^{\neq}$) was determined, see Table 1. The free energy of activation for **1** was

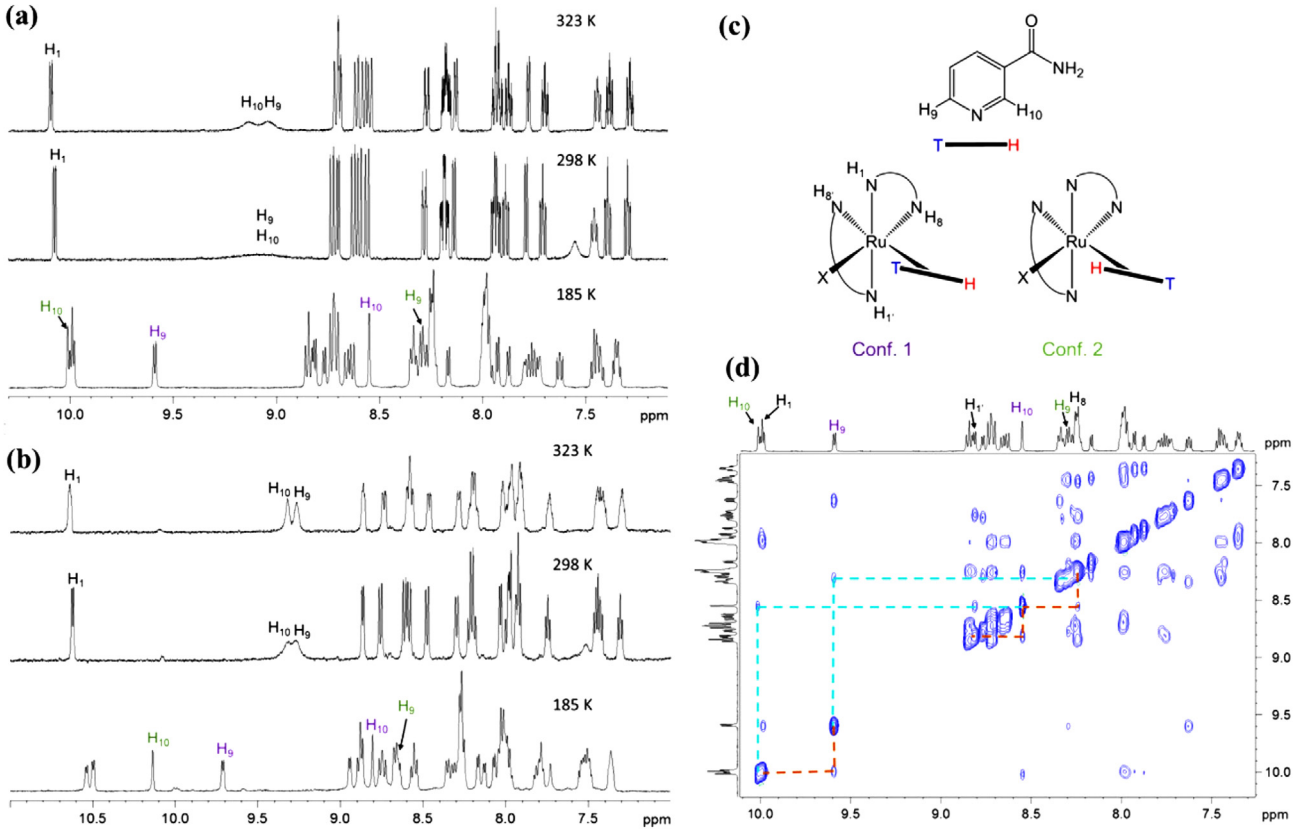

Fig. 3. Variable temperature ^{1}H NMR spectra (500 MHz) of *cis*-[Ru(bpy)$_2$(NA)Cl][PF$_6$] (**1**) (a) and *cis*-[Ru(bpy)$_2$(NA)I][PF$_6$] (**2**) (b) in acetone-d^6 at 323 K, 298 K and 185 K; (c) Structure and nomenclature of the atropisomers of *cis*-[Ru(bpy)$_2$(NA)X]$^+$ detected at 185 K; (d) ^{1}H–^{1}H NOESY spectrum (500 MHz) of *cis*-[Ru(bpy)$_2$(NA)Cl][PF$_6$] (**1**) in acetone-d^6 at 185 K, where blue lines represent exchange cross-peaks and orange lines represent NOE cross-peaks.

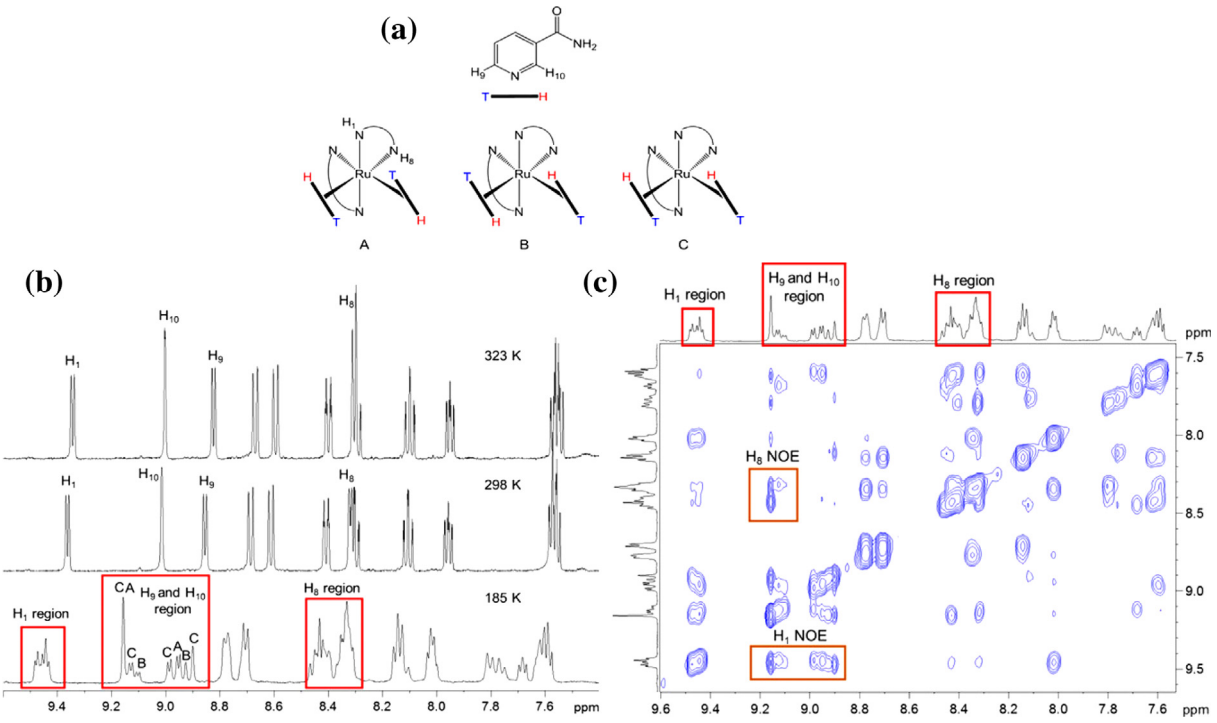

Fig. 4. (a) The nomenclature to describe the atropisomers; (b) Variable temperature ^{1}H NMR spectra (500 MHz) of *cis*-[Ru(bpy)$_2$(NA)$_2$][PF$_6$]$_2$ (**3**) in acetone-*d*^{6} at 323 K, 298 K and 185 K; (c) ^{1}H–^{1}H NOESY spectrum of **3** in acetone-*d*^{6} at 185 K.

3.9 kJ mol^{-1} higher than for **2**. These results suggested that the halide ligand was interacting with the aromatic protons of the monodentate ligand (H_9 and H_{10}), so hindering rotation at ambient temperature.

For the *bis*-NA complex **3**, the resonances of the NA ligand protons did not shift with increasing temperature (up to 323 K). However upon lowering the temperature to 185 K, a complex spectrum was obtained owing to the presence of 3 atropisomers (denoted A, B and C, Fig. 4a and b). At such low temperatures the NA ligand is held in one place (on the NMR timescale) for each atropisomer, and its orientation can be described by assigning H_{10} as the "head group", or H, and H_9 as the "tail", or T. The atropisomers were assigned by analysing the NOE interactions between H_{10}/H_9 with H_1/H_8 (Fig. 4c). For atropisomers A and B, there was only one environment for each H_{10} and H_9, thus there was one peak for each. For atropisomer A, H_{10} showed an NOE interaction with H_1 and H_8, and H_9 showed an NOE interaction with H_1. For atropisomer B, H_9 showed an NOE interaction with H_1 and H_8, and H_{10} showed an NOE interaction with H_1. In the case of atropisomer C, there are two environments for H_{10} and two for H_9, thus four peaks are observed for these protons. The ratios and chemical shifts of selected peaks for each atropisomer are given in Table S2. The chemical shift difference between H_{10} and H_9 did not change significantly between each atropisomer (~0.2 ppm). Whether H_{10} or H_9 is shifted downfield is dependent on the orientation of the NA ligand. Atropisomer C is the most

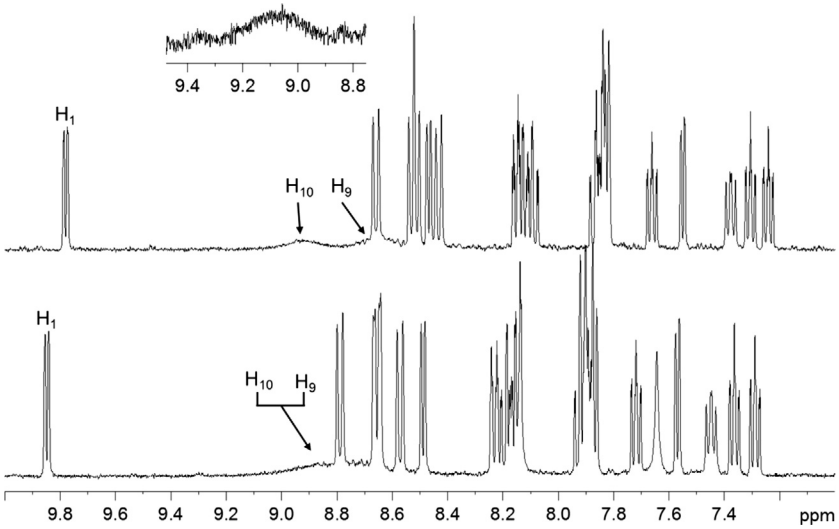

Fig. 5. ^{1}H NMR spectrum (400 MHz) of *cis*-[Ru(bpy)$_2$(NA)Cl][PF$_6$] (**1**) in DMSO-*d*$_6$ (bottom) and with 20 μL D$_2$O added (top). Inset is part of ^{1}H NMR spectrum of **1** in acetone-d^6 at 298 K.

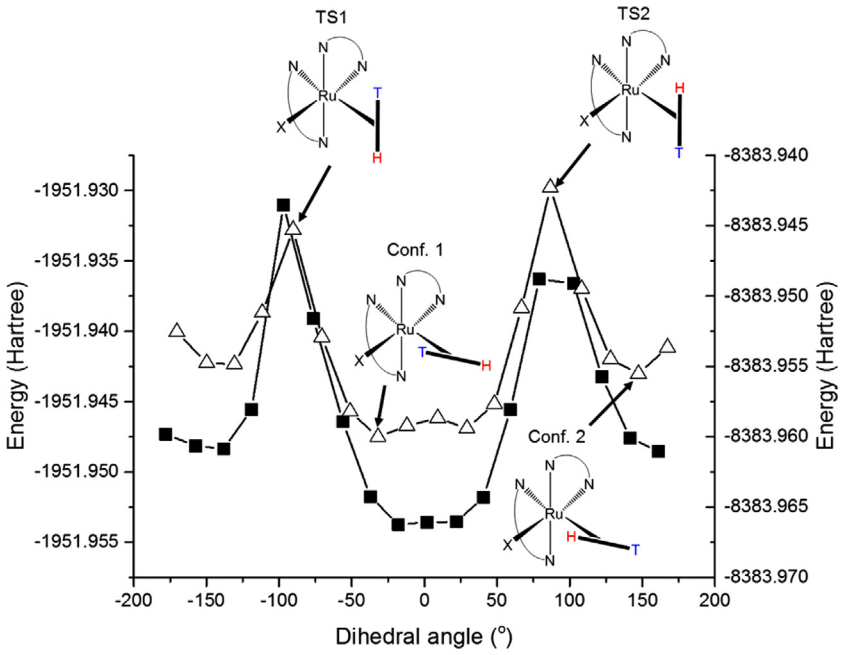

Fig. 6. Potential energy surface scan of *cis*-[Ru(bpy)$_2$(NA)Cl]$^+$ (**1**) (left axis and filled squares) and *cis*-[Ru(bpy)$_2$(NA)I]$^+$ (**2**) (right axis and empty triangles) using B3LPY/LanL2DZ/3-21G as the functional/basis set.

stable in solution, whereas atropisomer B is the least stable. These results suggested that the rotation of the monodentate ligands (NA) in complex **3** around the Ru–N axis was fast on the NMR timescale at 298 K and 323 K. However once the solution was cooled to 185 K, the NA ligands rotated much more slowly on the NMR timescale allowing atropisomers to be detected.

3.3. Solvent effect on dynamic behavior studied by ^{1}H NMR

In order to understand the nature of the conformational exchange, complexes **1** and **2** were dissolved in various deuterated solvents. For complex **1** in DMSO-d_6, the broad peak (H_9, H_{10} form NA) and the bpy H_1 proton has chemical shifts of 9.07 and 10.08 ppm, respectively, but in acetone-d^6 shifted upfield to 8.76 and 9.85 ppm. When a drop of D_2O was added to the DMSO-d_6 sample, the broad peak split into two peaks with chemical shifts of 8.92 and 8.64 ppm, and again the bpy H_1 proton shifted further upfield to 9.78 ppm, see Fig. 5. For **2** in DMSO-d_6, the broad peaks previously at 9.32 and 9.27 ppm in acetone-d^6 began to separate and shift upfield to 9.09 and 8.97 ppm, see Fig. S2. Similarly the bpy H_1 peak at 10.62 ppm in acetone-d^6 shifted upfield to 10.39 ppm in DMSO-d_6. These results show that more polar solvents (e.g. DMSO-d_6 and D_2O), disrupt the interaction leading to more resolved peaks for H_9 and H_{10}, consistent with the presence of hydrogen bonding.

3.4. Dynamic behavior studied by DFT

DFT was used to investigate whether an intramolecular interaction is the cause for the hindered rotation of the NA ligand at 298 K for **1** and **2**. A potential energy scan was performed to investigate the starting geometries and transition states by changing the dihedral angle between the halide and H_9, shown in Fig. 6. The lowest energy geometries were found to be Conf. 1 and Conf. 2. The conformation with the lowest energy was Conf. 1. There were two transition states, labelled transition state 1 (TS1) and transition state 2 (TS2), with TS2 having the highest energy. Geometry optimisations were performed to provide accurate energies of the conformations using two different functionals; B3LYP and PBE0. The DFT free energy of activation ($\Delta G^{\neq}_{DFT}$) was calculated as described in the Experimental Section 2, see Table 2. Generally the free energies of activation associated with **1** are greater than those for **2**. From exploring the ground state configurations and transition states, the main geometrical differences between **1** and **2** occur between the ground state configurations. Thus from here onwards only Conf. 1 and Conf. 2 will be discussed. The bond distance between H_{10}/H_9 and the halide X was investigated (H···X), see Table 3. Both PBE0 and B3LYP functionals showed that Conf. 1 had a shorter H_9/H_{10}···X distance than Conf. 2 by ~0.1 Å for both **1** and **2**. Additionally, both atropisomers of **1** had shorter H_9/H_{10}···X bond distances than both atropisomers of **2**. This is evident when visualising Conf. 1 of both **1** and **2** as the NA ligand appears to orientate itself closer to the halide for **1**, see Fig. 7. The DFT results correlate well with the experimental

Table 2
Free energy of activation ($\Delta G^{\neq}_{DFT}$) calculated from geometry optimised DFT structures of *cis*-[Ru(bpy)$_2$(NA)Cl]$^+$ (**1**) and *cis*-[Ru(bpy)$_2$(NA)I]$^+$ (**2**).

	$\Delta G^{\neq}_{DFT}$ (kJ mol^{-1})				
	Functional/basic set	Conf1 →TS1	Conf1 →TS2	Conf2 →TS1	Conf2 →TS2
1	B3LYP/LanL2DZ/6-31G**+	46.54	50.02	36.73	40.20
	PBE0/LanL2DZ/6-31G**+	50.17	54.09	40.59	44.50
2	B3LYP/LanL2DZ/6-31G**+	41.08	44.34	32.58	35.83
	PBE0/LanL2DZ/6-31G**+	45.53	49.37	37.45	41.29

Table 3
Bond distance H_{10}/H_9···X from geometry optimised DFT structures of complexes **1** and **2**.

		H_{10}/H_9···X distance (Å)	
		B3LYP/LanL2DZ/6-31G**+	PBE0/LanL2DZ/6-31G**+
1	Conf.1	2.43	2.44
	Conf.2	2.56	2.53
2	Conf.1	2.90	2.86
	Conf.2	3.02	2.97

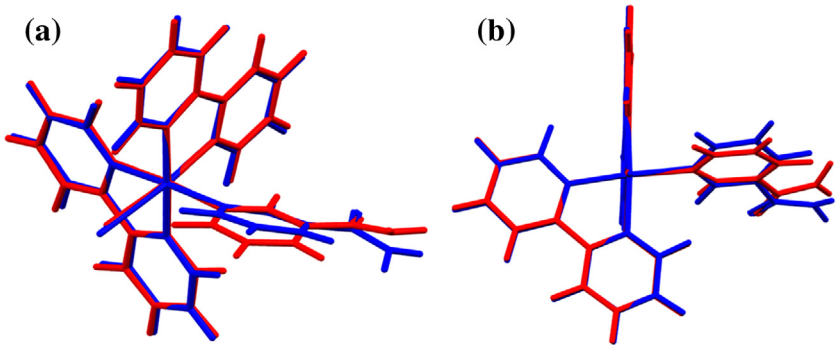

Fig. 7. Overlay of geometry optimised DFT structures (PBE0/LanL2DZ/6-31G**+) of $[Ru(bpy)_2(NA)Cl]^+$ (**1**) (red) and $[Ru(bpy)_2(NA)I]^+$ (**2**) (blue) to show orientation of NA ligand from two different angles, with (B) looking down the X–Ru bond. (For interpretation of the references to color in this figure legend, the reader is referred to the web version of this article.)

results, with the PBE0 functional performing the best. PBE0 has been shown to predict hydrogen bond energies well [24], however both functional showed that the free energy of activation was greater for **1** when compared to **2**. This can be attributed to the greater acceptor ability of Cl when compared to I; thus for **1** the rotation of the NA ligand was more hindered. This was further supported by the fact that the NA ligand orientates itself closer to the halide in **1**, as shown by the DFT geometry.

4. Conclusion

Two nicotinamide Ru(II) polypyridyl halide complexes, *cis*-$[Ru(bpy)_2(NA)Cl]^+$ (**1**), *cis*-$[Ru(bpy)_2(NA)I]^+$ (**2**) and one Ru(II)polypyridyl *bis*-substituted complex, *cis*-$[Ru(bpy)_2(NA)_2]^{2+}$ (**3**) were synthesised and characterized. The dynamic behavior of their atropisomers was demonstrated by temperature-dependent ^1H NMR spectroscopy which revealed hindered rotation of NA in the chlorido complex **1** and iodido complex **2** at ambient temperature. Interestingly the chlorido ligand hindered rotation more than the iodido, consistent with the heightened capability of the chlorido complex for hydrogen bonding interactions. However, NA in complex **3** rotated freely on the NMR timescale at 298 K. The hindered rotation was also explored by DFT calculations which suggested that this phenomenon was due to hydrogen bonding between the NA protons closest to the nitrogen of the pyridine ring and the halide. These complexes may be useful for the photoactivated delivery of the antibacterial agent nicotinamide, as part of a possible strategy to combat antimicrobial resistance, and dynamic processes within the complexes may have an influence on target recognition (e.g. membrane proteins).

5. Dedication

This article is dedicated to the memory of Karen Brewer, whose pioneering work on metal coordination complexes will ever be remembered.

Acknowledgments

We thank the ERC (Grant no. 247450), EPSRC (Grant no. EP/F034210/1), and the Royal Society (Newton International Fellowship for PZ) for support. L.S. thanks the Spanish Ministry of Economy and Competitiveness (Grant CTQ2012-39315 and Ramón y Cajal Fellowship RYC-2011-07787) and the MC CIG fellowship UCnanomat4iPACT (Grant no. 321791). We thank Dr Ivan Prokes for excellent assistance with NMR spectroscopy.

Appendix A. Supplementary data

Supplementary data associated with this article can be found, in the online version, at http://dx.doi.org/10.1016/j.ica.2016.06.014.

References

[1] V.P. Torchilin, Eur. J. Pharm. Sci. 11 (Supplement 2) (2000) S81–S91.
[2] J. Reedijk, Proc. Natl. Acad. Sci. 100 (7) (2003) 3611–3616.
[3] G.L. Patrick, An Introduction to Medicinal Chemistry, 5th ed., Oxford University Press, Oxford, UK, 2013.
[4] E.R. Jamieson, S.J. Lippard, Chem. Rev. 99 (9) (1999) 2467–2498.
[5] A.H. Velders, H. Kooijman, A.L. Spek, J.G. Haasnoot, D. de Vos, J. Reedijk, J. Inorg. Chem. 39 (14) (2000) 2966–2967.
[6] A.H. Velders, A.G. Quiroga, J.G. Haasnoot, J. Reedijk, Eur. J. Inorg. Chem. 2003 (4) (2003) 713–719.
[7] A.H. Velders, A.C.G. Hotze, G.A.V. Albada, J.G. Haasnoot, J. Reedijk, J. Inorg. Chem. 39 (18) (2000) 4073–4080.
[8] J. Clayden, W.J. Moran, P.J. Edwards, S.R. LaPlante, Angew. Chem. Int. Ed. 48 (35) (2009) 6398–6401.
[9] H.J. Maple, R.A. Garlish, I. Whitcombe, A. Hold, C.E. Prosser, D. Ford, H. Mackenzie, J. Crosby, J. Porter, R.J. Taylor, M.P. Crump, Anal. Chem. 85 (12) (2013) 5958–5964.
[10] S.R. LaPlante, P. Forgione, C. Boucher, R. Coulombe, J. Gillard, O. Hucke, A. Jakalian, M.-A. Joly, G. Kukolj, C. Lemke, R. McCollum, S. Titolo, P.L. Beaulieu, T. Stammers, J. Med. Chem. 57 (5) (2013) 1944–1951.
[11] W.M. Welch, F.E. Ewing, J. Huang, F.S. Menniti, M.J. Pagnozzi, K. Kelly, P.A. Seymour, V. Guanowsky, S. Guhan, M.R. Guinn, D. Critchett, J. Lazzaro, A.H. Ganong, K.M. DeVries, T.L. Staigers, B.L. Chenard, Bioorg. Med. Chem. Lett. 11 (2) (2001) 177–181.
[12] B.P. Sullivan, D.J. Salmon, T. Meyer, J. Inorg. Chem. 17 (12) (1978) 3334–3341.
[13] F. Dwyer, H. Goodwin, E. Gyarfas, Aust. J. Chem. 16 (4) (1963) 544–548.
[14] J. Sandstrom, Dynamic NMR Spectroscopy, 1st ed., Academic Press, London, 1982.
[15] M. Gielen, R. Willem, B. Wrackmeyer, Fluxional Organometallic and Coordination Compounds, John Wiley & Sons, West Sussex, UK, 2004.
[16] M. Pons, O. Millet, Prog. Nucl. Magn. Reson. Spectrosc. 38 (4) (2001) 267–324.
[17] M.J. Frisch, G.W. Trucks, H.B. Schlegel, G.E. Scuseria, M.A. Robb, J.R. Cheeseman, J.A. Montgomery, T. Vreven Jr., K.N. Kudin, J.C. Burant, J.M. Millam, S.S. Iyengar, J. Tomasi, V. Barone, B. Mennucci, M. Cossi, G. Scalmani, N. Rega, G.A. Petersson, H. Nakatsuji, M. Hada, M. Ehara, K. Toyota, R. Fukuda, J. Hasegawa, M. Ishida, T. Nakajima, Y. Honda, O. Kitao, H. Nakai, M. Klene, X. Li, J.E. Knox, H. P. Hratchian, J.B. Cross, C. Adamo, J. Jaramillo, R. Gomperts, R.E. Stratmann, O. Yazyev, A.J. Austin, R. Cammi, C. Pomelli, J.W. Ochterski, P.Y. Ayala, K. Morokuma, G.A. Voth, P. Salvador, J.J. Dannenberg, V.G. Zakrzewski, S. Dapprich, A.D. Daniels, M.C. Strain, O. Farkas, D.K. Malick, A.D. Rabuck, K. Raghavachari, J.B. Foresman, J.V. Ortiz, Q. Cui, A.G. Baboul, S. Clifford, J. Cioslowski, B.B. Stefanov, G. Liu, A. Liashenko, P. Piskorz, I. Komaromi, R.L. Martin, D.J. Fox, T. Keith, M.A. Al-Laham, C.Y. Peng, A. Nanayakkara, M. Challacombe, P.M.W. Gill, B. Johnson, W. Chen, M.W. Wong, C. Gonzalez, J.A. Pople, Gaussian 03, Gaussian Inc., Pittsburgh PA, 2003.
[18] A.D. Becke, J. Chem. Phys. 98 (7) (1993) 5648–5652.
[19] C. Lee, W. Yang, R. Parr, Phys. Rev. B 37 (2) (1988) 785–789.
[20] P.J. Hay, W.R. Wadt, J. Chem. Phys. 82 (1) (1985) 270–283.
[21] J.S. Binkley, J.A. Pople, W.J. Hehre, J. Am. Chem. Soc. 102 (3) (1980) 939–947.
[22] C. Adamo, V. Barone, J. Chem. Phys. 110 (13) (1999) 6158–6170.
[23] A.D. McLean, G.S. Chandler, J. Chem. Phys. 72 (10) (1980) 5639–5648.
[24] Y. Zhao, D.G. Truhlar, J. Chem. Theory Comput. 1 (3) (2005) 415–432.